

First principles investigation on Li or Sn codoped hexagonal tungsten bronzes as the near-infrared shielding material

Bo-Shen Zhou(周博深), Hao-Ran Gao(高浩然), Yu-Chen Liu(刘雨辰), Zi-Mu Li(李子木),Yang-Yang Huang(黄阳阳), Fu-Chun Liu(刘福春), and Xiao-Chun Wang(王晓春)

Citation: Chin. Phys. B, 2022, 31 (**5**): 057804. DOI: 10.1088/1674-1056/ac598a
Journal homepage: http://cpb.iphy.ac.cn; http://iopscience.iop.org/cpb

What follows is a list of articles you may be interested in

Quantum plasmons in the hybrid nanostructures of double vacancy defected graphene and metallic nanoarrays

Rui Tang(唐睿), Yang Xu(徐阳), Hong Zhang(张红), and Xin-Lu Cheng(程新路)
Chin. Phys. B, 2021, 30 (**1**): 017804. DOI: 10.1088/1674-1056/abaedb

A theoretical study on chemical ordering of 38-atom trimetallic Pd-Ag-Pt nanoalloys

Songül Taran, Ali Kemal Garip, Haydar Arslan
Chin. Phys. B, 2020, 29 (**7**): 077801. DOI: 10.1088/1674-1056/ab99b4

Tunable band gap and optical properties of surface functionalized Sc_2C monolayer

Shun Wang(王顺), Yu-Lei Du(杜宇雷), Wen-He Liao(廖文和)
Chin. Phys. B, 2017, 26 (**1**): 017806. DOI: 10.1088/1674-1056/26/1/017806

First-principles studies of electronic, optical, and mechanical properties of γ-$Bi_2Sn_2O_7$

Chao-Hao Hu(胡朝浩), Xue-Hui Yin(殷学辉), Dian-Hui Wang(王殿辉), Yan Zhong(钟燕), Huai-Ying Zhou(周怀营), Guang-Hui Rao(饶光辉)
Chin. Phys. B, 2016, 25 (**6**): 067801. DOI: 10.1088/1674-1056/25/6/067801

Linear optical properties of defective KDP with oxygen vacancy: First-principles calculations

Chen Xin, Zhao Qian-Qian, Wang Xiao-Chun, Chen Jun, Ju Xin
Chin. Phys. B, 2015, 24 (**7**): 077802. DOI: 10.1088/1674-1056/24/7/077802

First principles investigation on Li or Sn codoped hexagonal tungsten bronzes as the near-infrared shielding material

Bo-Shen Zhou(周博深)[1,2], Hao-Ran Gao(高浩然)[1,2], Yu-Chen Liu(刘雨辰)[1,2], Zi-Mu Li(李子木)[1,2], Yang-Yang Huang(黄阳阳)[1,2], Fu-Chun Liu(刘福春)[1,†], and Xiao-Chun Wang(王晓春)[1]

[1] *Institute of Atomic and Molecular Physics, Jilin University, Changchun* 130012, *China*
[2] *College of Physics, Jilin University, Changchun* 130012, *China*

(Received 16 June 2021; revised manuscript received 28 February 2022; accepted manuscript online 2 March 2022)

The 52% energy of the solar radiation is contributed by near-infrared radiation (NIR, 780–2500 nm). Therefore, the material design for the energy-saving smart window, which can effectively shield NIR and has acceptable visible transmittance, is vital to save the energy consumed on the temperature control system. It is important to find a non-toxic stable material with excellent NIR-shielding ability and acceptable visible transmittance. The systematic first-principles study on $Li_xSn_yWO_3$ ($x = 0, 0.33, 0.66$, and $y = 0, 0.33$) exhibits that the chemical stability is a positive correlation with the doping concentration. After doping, the Fermi-energy upshifts into the conduction band, and the material shows metal-like characteristics. Therefore, these structures $Li_xSn_yWO_3$ (except the structure with $x = 0.33$ and $y = 0$) show pronounced improvement of NIR shielding ability. Our results indicate that when $x = 0$ and $y = 0.33$, the material exhibits the strongest NIR-shielding ability, satisfying chemical stability, wide NIR-shielding range (780–2500 nm), and acceptable visible transmittance. This work provides a good choice for experimental study on NIR shielding material for the energy-saving window.

Keywords: density functional theory, electronic structure, near-infrared radiation shielding material

PACS: 78.20.−e, 88.40.fh, 95.85.Jq **DOI:** 10.1088/1674-1056/ac598a

1. Introduction

With higher demands for living quality, the expenditure of energy to maintain a comfortable indoor environment is ever-increasing. To control the indoor temperature within an appropriate interval, over 10% of total electricity consumption is consumed on air conditions and fans, and a corresponding amount of global greenhouse gas has been released.[1] Much good research has been performed on clean energy materials to decrease the greenhouse-gas emissions.[2–9] Thermal losses and solar irradiation through glass window account for 60% of the total energy expenditure of air-conditioned and heating systems.[10] Furthermore, solar radiation consists of roughly 5% ultraviolet radiation (UV, 10–400 nm), 43% visible radiation (400–780 nm), and 52% near-infrared radiation (NIR, 780–2500 nm),[11] which implies that the NIR spectrum accounts for the bulk source of thermal energy from the Sun. Therefore, with the expectation to reduce the emission of greenhouse gas, the utilization of new NIR-shielding material in green building areas is indispensable.

Some corresponding materials have attracted a lot of attention such as vanadium dioxide (VO_2),[12,13] rare-earth hexaboride nanoparticles (RB_6),[14,15] tin-doped indium oxide (ITO),[16,17] and hexagonal tungsten bronze (HTB).[18–25] However, VO_2 shows poor transmittance (30%)[13] in the visible light range. RB_6 (transmittance over 50% in the 2000–2500 nm range)[15] and ITO (near 0 absorption coefficient in 780–1000 nm)[16,17] shields only part of NIR which indicates that the NIR-shielding ability is limited. Although the Cs_xWO_3[26] exhibits a wide NIR shielding range and acceptable transmittance in the visible light range, it also exhibits chromatic instabilities when heated in a humid environment or being exposed to strong ultraviolet (UV) light, which renders detrimental effects on its long-life commercial application. Recently Sn_xWO_3 was reported as a non-toxic theranostic agent for imaging-guided cancer therapy, because of its absorption ability of NIR.[25] However, compared with the Cs_xWO_3, the NIR-shielding ability of Sn_xWO_3 is not so satisfying (transmittance over 20% in the near-infrared range). Therefore, there is a necessity to find a less toxic, and chromatic stable material simultaneously with a wide NIR-shielding range and acceptable visible transmittance.

Among these materials, HTB exhibits high visible light transmissivity and a wide NIR-shielding range (780–2500 nm). Recent studies have revealed the changing mechanism of the optical properties of HTB, which is highly correlated with the band structures and concentration of free carriers. In more detail, when photons in the NIR spectrum irradiate these materials, the photons could be absorbed to complete the transition of electrons in the valence bands (VBs) to the conductor bands (CBs).[19,27] On the other hand, the localized surface plasma resonance (LSPR) can be induced by the aggregated free electrons in the CBs to shield the near-infrared ray.[27–29] In recent research, it was found that the empty trigonal cavity could be occupied by light metallic elements, e.g., Li.[19,30] Therefore, there is a possibility to improve the NIR-shielding ability of materials by inserting Li and Sn atoms at

†Corresponding author. E-mail: lfc@jlu.edu.cn

© 2022 Chinese Physical Society and IOP Publishing Ltd

trigonal and hexagonal cavities of HTB, respectively, which renders the rise of free carrier concentration in materials. As far as I know, rare studies have reported $Li_xSn_yWO_3$ as one of the promising materials for the future energy-saving window.

In this work, the $Li_xSn_yWO_3$ was investigated using density functional theory (DFT). First and foremost, the geometry structures of $Li_xSn_yWO_3$ with six different doping concentrations had been constructed. Thereafter, binding energy was calculated for comparing the chemical stability of these structures. To further illustrate the thermal stability, the molecular dynamics study of $Sn_{0.33}WO_3$ was performed. And then, the electronic properties of structures were investigated for a better understanding of the changing of optical properties. Finally, the optical properties of $Li_xSn_yWO_3$ were calculated considering local field effects based on the random-phase approximation (RPA).[31] The results show that when $y = 0$ the NIR shielding ability increased with the x increase, and when $y = 0.33$ the NIR shielding ability first increases and then decreases with the x increase. When $x = 0$ and $y = 0.33$, the material exhibits the strongest NIR-shielding ability, is less toxic, has satisfying chemical stability, wide NIR-shielding range (780–2500 nm), and an acceptable visible transmittance which means it can be applied on the future energy-saving smart window.

2. Calculational method

In this paper, all calculation results were obtained via the Vienna *ab initio* simulation package (VASP).[32] We employed the generalized gradient approximation (GGA) with the Perdew–Burke–Ernzerh (PBE).[33] and used the projector augmented wave (PAW)[34] method. The influence of spin–orbit coupling effect (SOC) on electronic and optical properties was concerned. The valence electrons configurations for O, W, Li, Sn atoms were $2s^22p^4$, $5d^46s^2$, $2s^1$ and $5s^25p^2$, respectively. We adopted a Brillouin zone of $9 \times 9 \times 15$ with a Γ centered Monkhorst–Pack k-point mesh with cut-off energy of 500 eV during geometry optimization. And all of the structures were relaxed until the force on each atom was less than 0.02 eV/Å. And molecular dynamics simulations were performed at the time step of 2 fs, canonical ensemble (NVT), on the $2 \times 2 \times 2$ supercell at the temperature of 300 K. Self-consistent computations were performed with a convergence criterion of 10^{-8} eV in energy. And the optical properties were concerned with approximation including local field effects in the RPA.[31] When calculating optical properties, nearly 100 bands were set to ensure that the empty bands were included in the calculations.

3. Results and discussion

3.1. Geometry structures and thermal stability

Table 1 shows the lattice parameters of optimized h-WO_3, which were in accord with previous experimental results (x-ray diffraction data of h-WO_3 with a space group of *P6/mmm* (No. 191)).[35]

Table 1. Calculated and experimental crystal structure parameters of h-WO_3.

	a (Å)	b (Å)	c (Å)
Cal. WO_3	7.45	7.45	3.83
Exp. WO_3[36]	7.30	7.30	3.90

In this research, six structures of $Li_xSn_yWO_3$ (with $x = 0$, 0.33 or 0.66; $y = 0$ or 0.33) were concerned. For each structure, all spatial arrangements for Sn and Li atoms were considered, and only the most stable one was singled out as representative of every structure. Then, the binding energy of those six structures was calculated as below:

$$E_b = E_{total} - E_{WO_3} - n_{Li}E_{Li} - n_{Sn}E_{Sn}, \quad (1)$$

where E_{total} is the total energy of the system, E_{WO_3} is the energy of the pure h-WO_3, n_{Li} is the number of the Li atoms, E_{Li} is the energy of the isolated Li atom, n_{Sn} is the number of the Sn atoms, and E_{Sn} is the energy of the isolated Sn atom. In Fig. 2, it was found that the binding energy declines while the x and y increase. As is well known, this indicates the increase of stability. The energy evolution of the 10 ps MD simulation of $Sn_{0.33}WO_3$ under the room temperature was exhibited in Fig. 3. And the average energy of each atom was nearly a constant. This means $Sn_{0.33}WO_3$ is stable at room temperature.

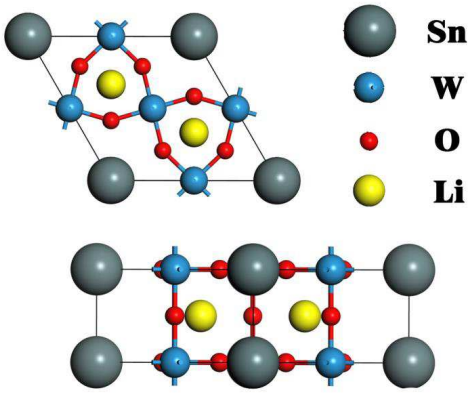


Fig. 1. The top view and side view of $Li_{0.66}Sn_{0.33}WO_3$.

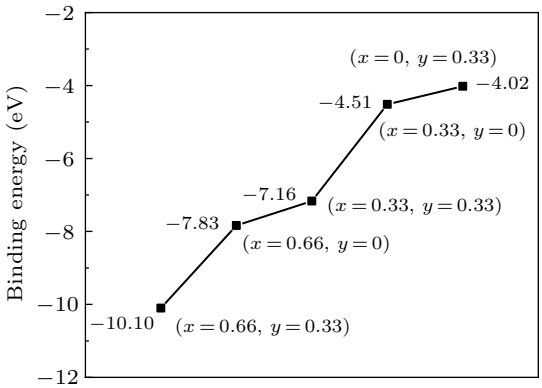


Fig. 2. The binding energy of $Li_xSn_yWO_3$ ($x = 0, 0.33, 0.66$; $y = 0, 0.33$).

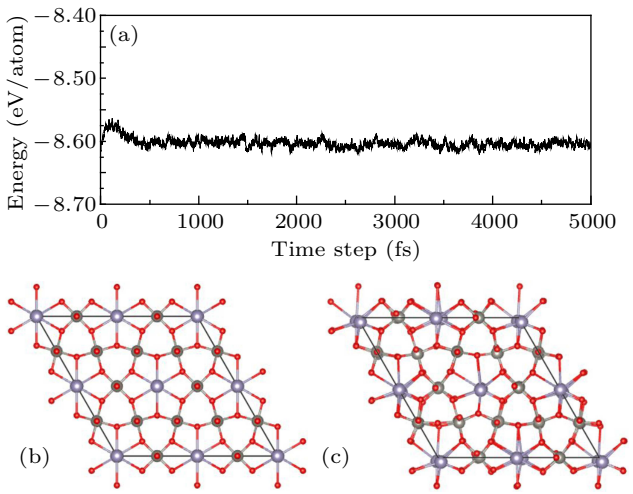


Fig. 3. (a) The energy evolution of $Sn_{0.33}WO_3$ during 10 ps MD simulations at room temperature, (b) and (c) are the structures before and after MD simulations.

3.2. Electronic structure

In Fig. 4, it was found that h-WO_3 is an indirect bandgap semiconductor since whose valence band maximum (VBM) and conduction band minimum (CBM) do not at the same point, which occurs at *A* point and *Γ* point, respectively. The calculated bandgap of h-WO_3 is 0.44 eV, which approaches the previous result,[37] as results obtained through DFT theory are always underestimated. The band structure after doping is very similar to the pure h-WO_3. Besides, it is found that the Fermi energy has been upshifted into the conduction bands (CBs) and the electrons occupied the bands that were empty before.

The density of states of $Li_xSn_yWO_3$ is shown in Fig. 5. The DOS of pure h-WO_3 is in line with Liu's result.[18] For pure h-WO_3, the valence bands (VBs) mainly consist of the O-2p states, and the conduction bands (CBs) are mainly composed of the W-5d states, which are consistent with the experimental characterizations.[38] Since one W atom is surrounded by six O atoms forming an octahedral structure, W-5d states are split into t_{2g} (low energy) and e_g (high energy) states,[39,40] which could be observed through several peaks shown on PDOS curves of h-WO_3, contributed from W-5d states. And the strong hybridization between O-2p states and W-5d states also indicates a strong covalency of the bonding. On the one hand, when Sn is doped in the h-WO_3, the Fermi energy is upshifted in the conduction band, and the material exhibits the metal-like behavior, while electrons in Sn-5p mainly act as the free electrons. As the result, the materials display the n-type electronic conductivity. On the other hand, albeit Li-2s states are nearly zero, once Li is doped into h-WO_3, the Fermi energy was upshifted, which improves the free carrier concentration of the material. In more detail, as shown in Table 2, it was found that the more ions are doped, the higher the free carrier concentration of the material will be. Compared with other structures, the free carrier concentration of $Li_{0.33}WO_3$ is rather low, which is the reason why its NIR-shielding ability is almost zero.

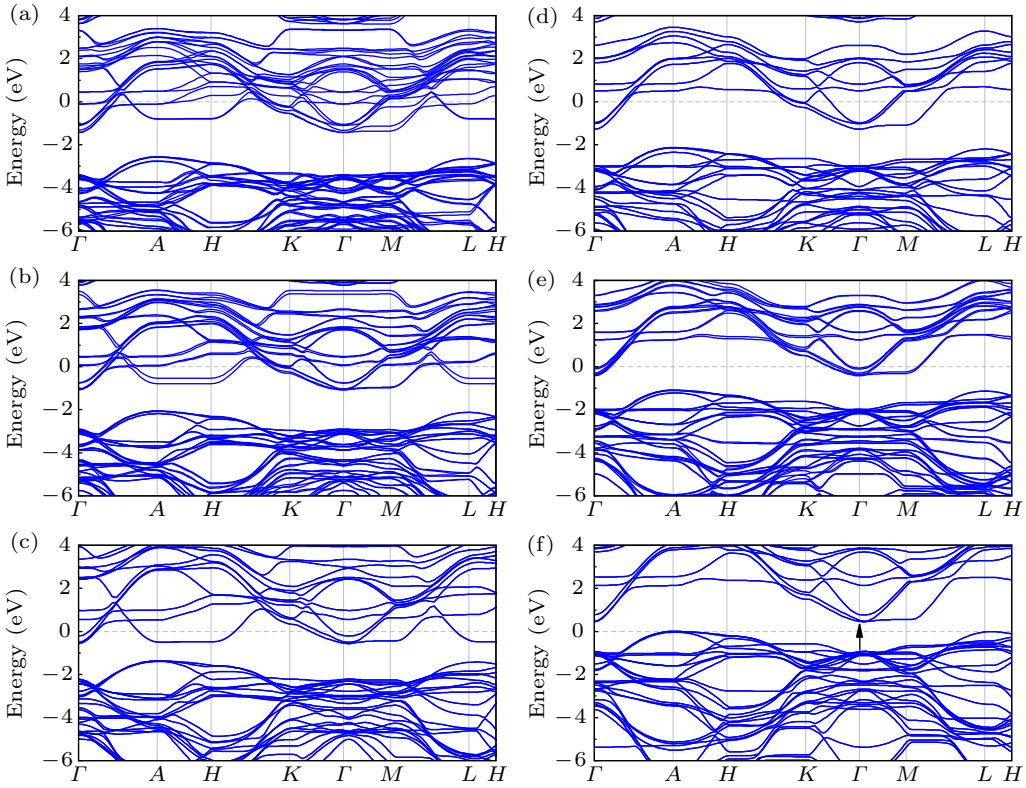


Fig. 4. The band structures of (a) $Li_{0.66}Sn_{0.33}WO_3$, (b) $Li_{0.33}Sn_{0.33}WO_3$, (c) $Sn_{0.33}WO_3$, (d) $Li_{0.66}WO_3$, (e) $Li_{0.33}WO_3$ and (f) WO_3.

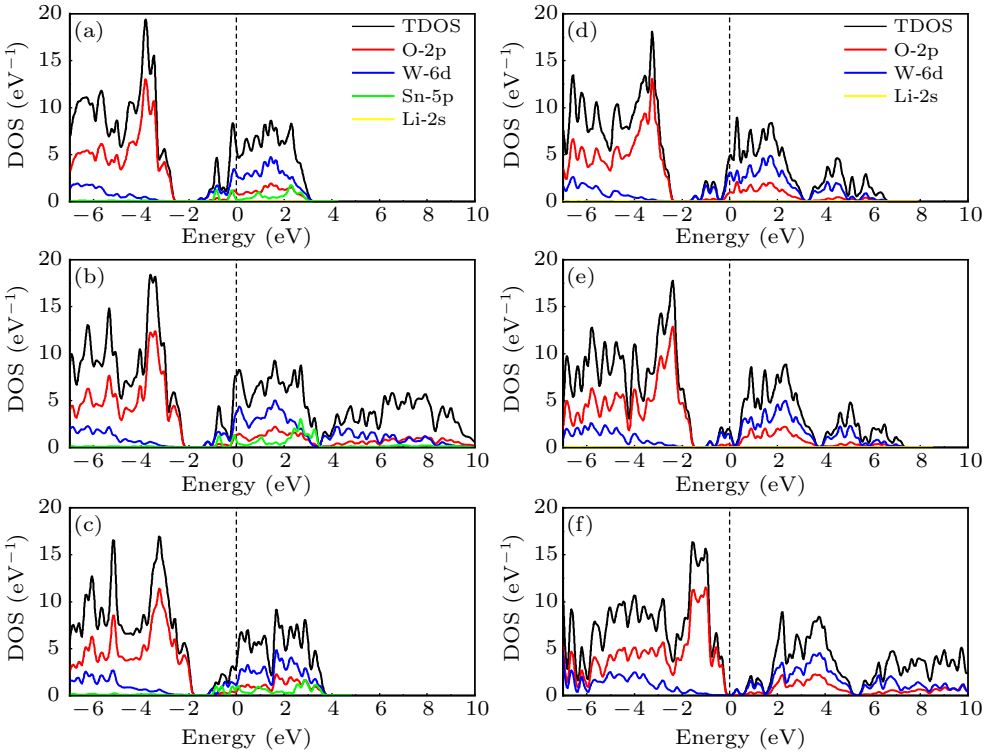


Fig. 5. The total density of states (TDOS) and project density of states (PDOS) of (a) $Li_{0.66}Sn_{0.33}WO_3$, (b) $Li_{0.33}Sn_{0.33}WO_3$, (c) $Sn_{0.33}WO_3$, (d) $Li_{0.66}WO_3$, (e) $Li_{0.33}WO_3$ and (f) WO_3. The Fermi energy level is indicated by the vertical dashed lines at energy equal to zero.

Table 2. Free carrier concentration and binding energy of five structures.

Doping concentration	Free carrier concentration (10^{22} cm^{-3})	Binding energy (eV)
$x = 0.66, y = 0.33$	2.00	−10.10
$x = 0.33, y = 0.33$	1.50	−7.16
$x = 0, y = 0.33$	1.06	−4.02
$x = 0.66, y = 0$	0.99	−7.83
$x = 0.33, y = 0$	0.49	−4.51

Besides, the codes behind the effects of doping Sn and Li atoms on the enhancement of free carrier concentration have been trying to decipher, which are crucial to understanding the changes in the NIR-shielding ability of various structures of $Li_xSn_yWO_3$. The number of free carriers (N) is given by Eq. (2), where $f(E)$ is the Fermi–Dirac distribution and $g(E)$ is the density of states. At 0 K, the Fermi–Dirac distribution for electrons would simplify to either 0 ($E > E_f$) or 1 ($E < E_f$). Although this assumption is only completely accurate at 0 K, the total concentration should relatively remain unchanged when temperature build-up. Therefore Eq. (2) can be simplified to Eq. (3), where the V is the unit cell volume and the E_c is the bottom of the conduction band.[41]

$$N(E) = \int f(E)\, g(E)\, \mathrm{d}E, \tag{2}$$

$$N = nV = \int_{E_c}^{E_f} g(E)\, \mathrm{d}E. \tag{3}$$

3.3. Optical properties

In this investigation, the imaginary part of the dielectric function was concerned with the local field in the random-phase approximation (RPA).[31] And the real part of the dielectric function was calculated through the Kramer–Kronig relation. The reflectivity R, absorption coefficient α, and transmittance T could be derived from the dielectric function by the following formula:[18,42,43]

$$R(\omega) = \left| \frac{\sqrt{\varepsilon_1(\omega) + \mathrm{i}\varepsilon_2(\omega)} - 1}{\sqrt{\varepsilon_1(\omega) + \mathrm{i}\varepsilon_2(\omega)} + 1} \right|^2, \tag{4}$$

$$\alpha(\omega) = \sqrt{2}\omega \left[\sqrt{\varepsilon_1^2(\omega) + \varepsilon_2^2(\omega)} - \varepsilon_1(\omega) \right]^{\frac{1}{2}}, \tag{5}$$

$$T(\omega) = \frac{[1 - R(\omega)]^2 \exp[-\alpha(\omega) d]}{1 - R^2(\omega) \exp[-2\alpha(\omega) d]}, \tag{6}$$

where d is the thickness of the film, which is 50 nm in this calculation, and ε_1 and ε_2 are real part and imaginary part of the dielectric function, respectively. For simplicity, only conditions concerning optical properties along with the x-axis of $Li_xSn_yWO_3$ are shown below.

To understand the change of optical properties, two models were introduced. The first model is the interband transition. In this module, the electrons can move or jump from a filled band to the higher empty band. The second is the intraband transition, which can describe the contribution of free carriers and always be concerned as the source of plasmonic resonances. And it always leads to a large of optical losses at low frequency.[44–46] In this model, the free carrier concentration plays a very important role. The dielectric function of intra-

band transition can be described by the Drude model[44,47,48]

$$\varepsilon^{\text{intra}} = 1 - \frac{\omega_p^2}{(\omega^2+\gamma^2)} + \mathrm{i}\frac{\omega_p^2\gamma}{\omega(\omega^2+\gamma^2)}, \tag{7}$$

where γ is the Drude relaxation rate, which is inverse with the mean free path of electrons,[49] and ω_p is the plasma frequency which is scales with the free carrier concentration.[14]

As shown in Fig. 6(b), the imaginary part of the dielectric function of h-WO_3 goes to zero when the energy approaches 0 eV, which is in line with the previous result.[19,50] The plasma energy where the intersection points between the gray line where the real part equals zero, is corresponding to a fast abatement of the reflectivity as shown in Fig. 7, respectively. In Fig. 6, when energy is less than 1, it can be found that with the increase of free carrier concentration, the imaginary part of the dielectric function increases first and then decreases, and the situation is quite reversed for the real part. This change is caused by the increase of free carrier concentrations and the decrease of the mean free path of electrons. The mean free path of electrons describes the average distance traveled by the electron. When the inserted atoms increase, the possibility of the electron being stopped by inserted ions increases. Therefore, the mean free path of electrons would decrease with the increase of doping concentration. And the Drude relaxation rate is inversed with the mean free path of electrons Therefore, when Li and Sn are codoped in the h-WO_3, although the free carrier concentration would increase with the doping concentration increasing, the Drude relaxation rate would also increase. This explains the decline of the NIR shielding ability with excessive doping concentration.

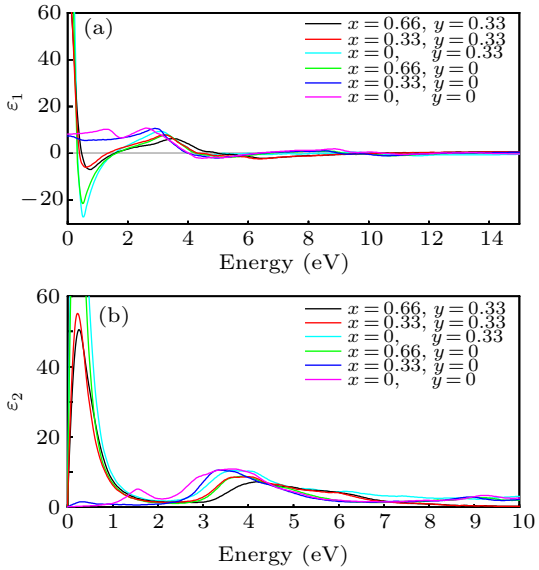


Fig. 6. The dielectric function of $Li_xSn_yWO_3$ ($x = 0, 0.33, 0.66$ and $y = 0, 0.33$) at approximation including local field effects in the RPA.

In Fig. 7, the h-WO_3 shows nearly no NIR-shielding ability, which corresponds with the previous result.[30] The absorption coefficient and reflectivity of $Sn_{0.33}WO_3$ sharply changed in the visible light range, which is also in good agreement with the experiment.[25] The peak of the absorption coefficient of h-WO_3 at 700 nm is originated due to the transition of electrons, which is in accordance with the transition between two bands in Fig. 4(f). For other structures, the Fermi energy upshifted, and the electron occupied the bands that were empty before. That is why the absorption peaks of other structures disappeared. Compared with ITO,[16,17] which shows nearly zero absorption coefficient in the range from 780–1000 nm, the absorption coefficient of $Sn_{0.33}WO_3$ is over 3×10^5 at 1000 nm. In Fig. 8, except the $Li_{0.33}WO_3$ is nearly the same as the h-WO_3, other structures show pronounced improvement of reflectivity.

Figure 9 shows the transmittance of $Li_xSn_yWO_3$ in the NIR and visible light range. The valley of transmittance of pure h-WO_3 can be found at 700 nm, which is according to the absorption coefficient and interband transition. The $Sn_{0.33}WO_3$ shows the strongest NIR shielding ability and acceptable transmittance at the visible light range. For $Sn_{0.33}WO_3$, the maximum visible transmittance is over 60%

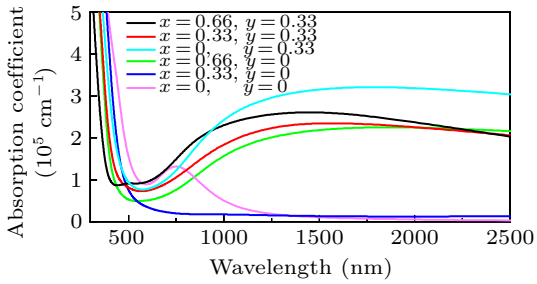


Fig. 7. The absorption coefficient of $Li_xSn_yWO_3$ ($x = 0, 0.33, 0.66$ and $y = 0, 0.33$) at approximation including local field effects in the RPA.

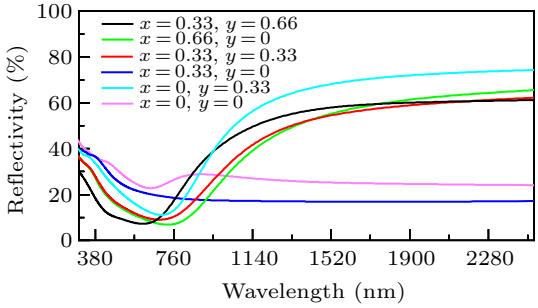


Fig. 8. The reflectivity of $Li_xSn_yWO_3$ ($x = 0, 0.33, 0.66$ and $y = 0, 0.33$) at approximation including local field effects in the RPA.

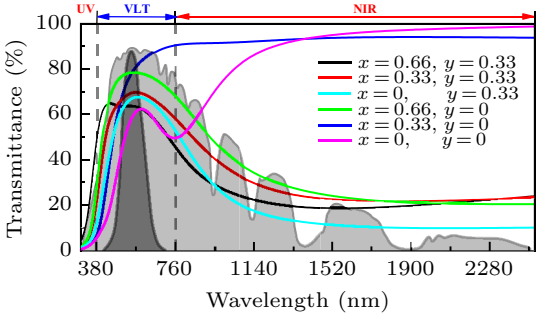


Fig. 9. Comparing the transmittance of $Li_xSn_yWO_3$. The grey and light gray areas indicate the global tilt and extraterrestrial reference solar spectrum (ISO 9845-1, 1992).

at 562 nm which is larger than the VO_2 (36.2%) and the minimum NIR transmittance is nearly 10% over 1000 nm which is very close to the VO_2.[13] The results show that the $Sn_{0.33}WO_3$ can be applied as excellent NIR-shielding material with acceptable visible transmittance.

4. Conclusions

In summary, the binding energy, electric structure, and optical properties of $Li_xSn_yWO_3$ were studied using the DFT calculation. After doping, the Fermi energy level entered into the conductor band and the electrons occupied the bands that were empty before doping, which indicates the metal-like characteristics of the doped material. The density of states shows that the Sn-5p electrons act as the free electrons in the conductor and Li-ions provide nearly no electron. Therefore, except the $Li_{0.33}WO_3$, other doped structures show metal-like characteristics. The optical properties show that except the $Li_{0.33}WO_3$ exhibiting poor NIR shielding ability, other materials show excellent visible transmittance and NIR-shielding. Our results show that $Sn_{0.33}WO_3$ is the material with satisfying chemical stability, excellent NIR-shielding ability, wide NIR-shielding range (780–2500 nm), and acceptable visible transmittance. It can be expected that our rational theoretical prediction should serve as an impetus for the pursuit of experimental realization of these (Li, Sn) codoped hexagonal tungsten bronze as NIR-shielding materials for the energy-saving smart window made in buildings.

Acknowledgment

Thanks to the Beijing Super Cloud Computing Center for assistance with calculation.

References

[1] Bechinger C, Ferrere S, Zaban A, Sprague J and Gregg B A 1996 *Nature* **383** 608
[2] Zhao Y Z, Jia H J, Zhao S N, Wang Y B, Li H Y, Zhao Z L, Wu Y X and Wang X C 2020 *Physica E* **117** 113817
[3] Yu H X, Mu H M, Zhu D R, Zhang Y, Wang X C and Zhang S 2019 *Int. J. Hydrogen Energ* **44** 19920
[4] Mu H m, Yu H X, Zhu D R, Zhao S N and Wang X C 2019 *Applied Surface Science* **498** 143823
[5] Li J P, Jia H J, Zhu D R, Wang X C, Liu F C and Yang Y J 2019 *Applied Surface Science* **463** 918
[6] Zhao L S, Chen C P, Liu L L, Yu H X, Chen Y and Wang X C 2018 *Chin. Phys. B* **27** 016301
[7] Jia H J, Mu H M, Li J P, Zhao Y Z, Wu Y X and Wang X C 2018 *Phys. Chem. Chem. Phys.* **20** 26288
[8] Zhao L S, Wang Y, Chen C P, Liu L L, Yu H X, Zhang Y, Chen Y and Wang X C 2017 *Physica E* **91** 82
[9] Liu L L, Chen C P, Zhao L S, Wang Y and Wang X C 2017 *Carbon* **115** 773
[10] Jelle B P, Hynd A, Gustavsen A, Arasteh D, Goudey H and Hart R 2012 *Solar Energy Materials and Solar Cells* **96** 1
[11] Levinson R, Berdahl P and Akbari H 2005 *Solar Energy Materials and Solar Cells* **89** 319
[12] Qazilbash M M, Brehm M, Chae B G, Ho P C, Andreev G O, Kim B J, Yun S J, Balatsky A, Maple M and Keilmann F 2007 *Science* **318** 1750
[13] Xiao L, Su Y, Qiu W, Ran J, Liu Y, Wu J, Lu F, Shao F and Peng P 2016 *Appl. Phys. Lett.* **109** 193906
[14] Chao L, Bao L, Wei W, O T and Zhang Z 2016 *J. Alloys Compd.* **672** 419
[15] Takeda H, Kuno H and Adachi K 2008 *J. Am. Chem. Soc.* **91** 2897
[16] Kanehara M, Koike H, Yoshinaga T and Teranishi T 2009 *J. Am. Chem. Soc.* **131** 17736
[17] Pattathil P, Giannuzzi R and Manca M 2016 *Nano Energy* **30** 242
[18] Xu Q, Xiao L, Ran J, Tursun R, Zhou G, Deng L, Tang D, Shu Q, Qin J, Lu G and Peng P 2018 *J. Appl. Phys.* **124** 193102
[19] Yang C, Chen J F, Zeng X, Cheng D and Cao D 2014 *Industrial & Engineering Chemistry Research* **53** 17981
[20] Guo C, Yin S, Sato T and Priya S 2012 *Journal of the American Ceramic Society* **95** 1634
[21] Lee Y, Lee T, Jang W and Soon A 2016 *Chemistry of Materials* **28** 4528
[22] Guo C, Yin S, Dong Q, Kimura T, Tanaka M, Hang le T, Wu X and Sato T 2013 *J. Nanosci. Nanotechnol.* **13** 3236
[23] Ran S, Liu J, Shi F, Fan C, Chen B, Zhang H, Yu L and Liu S H 2018 *Solar Energy Materials and Solar Cells* **174** 342
[24] Guo C, Yin S, Yan M and Sato T 2011 *Journal of Materials Chemistry* **21** 5099
[25] Gao Y, Wang F, Huang W, Yang C, Guo W, Song C, Zhang Q, Yang B, Xu Y and Guo C 2019 *Nanoscale* **11** 3300
[26] Adachi K, Ota Y, Tanaka H, Okada M, Oshimura N and Tofuku A 2013 *J. Appl. Phys.* **114** 194304
[27] Adachi K and Asahi T 2012 *Journal of Materials Research* **27** 965
[28] Naik G V, Shalaev V M and Boltasseva A 2013 *Adv. Mater.* **25** 3264
[29] Lang Z Z, Liu X Q and Chen X M 2021 *Chin. Phys. Lett.* **38** 047701
[30] Yang C, Chen J F, Zeng X, Cheng D, Huan H and Cao D 2016 *Nanotechnology* **27** 075203
[31] Gajdoš M, Hummer K, Kresse G, Furthmöller J and Bechstedt F 2006 *Phys. Rev. B* **73** 045112
[32] Kresse G and Hafner J 1994 *Phys. Rev. B* **49** 14251
[33] Perdew J P, Burke K and Ernzerhof M 1996 *Phys. Rev. Lett.* **77** 3865
[34] Vanderbilt D 1990 *Phys. Rev. B* **41** 7892
[35] Gerand B, Nowogrocki G, Guenot J and Figlarz M 1979 *Journal of Solid State Chemistry* **29** 429
[36] Cheng K, Jacobson A and Whittingham M 1981 *Solid State Ionics* **5** 355
[37] Ingham B, Hendy S C, Chong S V and Tallon J L 2005 *Phys. Rev. B* **72** 045112
[38] Khyzhun O Y, Solonin Y M and Dobrovolsky V 2001 *J. Alloys Compd.* **320** 1
[39] Goodenough J B 1971 *Progress in Solid State Chemistry* **5** 145
[40] Granqvist C G 2000 *Solar Energy Materials and Solar Cells* **60** 201
[41] Sheardy A T, Arvapalli D M and Wei J 2020 *Nanoscale Advances* **2** 1054
[42] Sun J, Wang H T, He J and Tian Y 2005 *Phys. Rev. B* **71** 125132
[43] Liu C, Shu Q, Qin J, Yuan Y, Qiu W, Peng P and Xiao L 2019 *AIP Advances* **9** 115014
[44] Kim J, Jhi S H and Ryeol Lee K 2011 *J. Appl. Phys.* **110** 083501
[45] Yang J Y, Xu M and Liu L H 2016 *Journal of Quantitative Spectroscopy and Radiative Transfer* **184** 111
[46] Mendoza-Galván A and González-Hernández J 2000 *J. Appl. Phys.* **87** 760
[47] Xue Y, Zhang Y and Zhang P 2009 *Phys. Rev. B* **79** 205113
[48] Yamada Y, Tajima K, Bao S, Okada M and Yoshimura K 2009 *Solid State Ionics* **180** 659
[49] Peña-Rodríguez O 2017 *J. Alloys Compd.* **694** 857
[50] Yang H, Sun H, Li Q, Li P, Song K, Song B and Wang L 2019 *Vacuum* **164** 411